ISSN 0016-8521, Geotectonics, 2017, Vol. 51, No. 6, pp. 535–548. © Pleiades Publishing, Inc., 2017.
Original Russian Text © V.G. Trifonov, S.Yu. Sokolov, 2017, published in Geotektonika, 2017, No. 6, pp. 3–17.

Sublithospheric Flows in the Mantle

V. G. Trifonov* and S. Yu. Sokolov

Institute of Geology, Russian Academy of Sciences, Moscow, 119017 Russia

**e-mail: trifonov@ginras.ru*

Received April 7, 2017

Abstract—The estimated rates of upper mantle sublithospheric flows in the Hawaii–Emperor Range and Ethiopia–Arabia–Caucasus systems are reported. In the Hawaii–Emperor Range system, calculation is based on motion of the asthenospheric flow and the plate moved by it over the branch of the Central Pacific plume. The travel rate has been determined based on the position of variably aged volcanoes (up to 76 Ma) with respect to the active Kilauea Volcano. As for the Ethiopia–Arabia–Caucasus system, the age of volcanic eruptions (55–2.8 Ma) has been used to estimate the asthenospheric flow from the Ethiopian–Afar superplume in the northern bearing lines. Both systems are characterized by variations in a rate of the upper mantle flows in different epochs from 4 to 12 cm/yr, about 8 cm/yr on average. Analysis of the global seismic tomographic data has made it possible to reveal rock volumes with higher seismic wave velocities under ancient cratons; rocks reach a depth of more than 2000 km and are interpreted as detached fragments of the thickened continental lithosphere. Such volumes on both sides of the Atlantic Ocean were submerged at an average velocity of 0.9–1.0 cm/yr along with its opening. The estimated rates of the mantle flows clarify the deformation properties of the mantle and regulate the numerical models of mantle convection.

Keywords: Hawaii–Emperor Range, Ethiopia–Arabia–Caucasus, eruption age, seismic tomography, sublithospheric flows, submergence of lithosphere fragments, mantle flow velocity

DOI: 10.1134/S0016852117060085

INTRODUCTION

Soon after the main postulates of lithospheric plate tectonics were formulated, the general mantle thermal convection was proposed as the driving force of plate motion [50]. E.V. Artyushkov [1, 2] and O.G. Sorokhtin [30] gave reasons for greater efficiency of the chemical density convection related to mantle differentiation. Over time, plate tectonics theory was modernized due to substantiation of the diffusive nature of plate boundaries [53], their tectonic layering [32], and transition of many subduction zones within the mantle transitional layer (about 400–700 km) to subhorizontal high-velocity lenses extending under continents. These lenses were called stagnating slabs [52, 59] or large mantle wedges [14]. At the current developmental stage of plate tectonics theory, convection in mantle and upper mantle flows as its derivatives are suggested as the leading driving forces of plate motion, but the nature of these processes is understood by the researchers in different ways.

Artyushkov [3, 4] suggests replacement of the lithosphere by the asthenospheric mantle as one of the factors of mountain formation and considers the lateral flow of the sublithospheric mantle a possible reason for nonuniformity of age of Late Cenozoic activation of vertical motions in the Central Asia Region. N.L. Dobretsov et al. [9–11] distinguish between lower-mantle and upper mantle convection, emphasizing the critical importance of the latter in the transformation and tectonic development of the lithosphere. Meanwhile, the above-mentioned authors note the difficulties arising from the assumption of the upper mantle convection under the continents, because the asthenosphere is occasionally dramatically reduced in thickness. L.I. Lobkovsky [22], while acknowledging general mantle convection, prioritizes the role of upper mantle convection in the Cenozoic tectonic development of the Northeastern Asia Region.

V.P. Trubitsyn [36–38, 71] carried out the numerical modeling for general mantle convection as the main driving force for upper mantle flows. The mantle convection results in separation and motion of lithospheric plates. The general mantle plumes (superplumes) were considered to be ascending convection branches, while subducting slabs were assumed to be related to descending branches. It should be noted that spreading and subduction zones can change their position over time, and oceanic spreading zones are fed by asthenospheric flows rather than by superplumes. The investigation involved analysis of the influence of the recent and ancient continental position on the thermal characteristics of convection and changes in the conditions and structure of mantle flows in the transitional mantle layer (410–670 km). Thickening of the D" layer up to 250–300 km in the mantle base

under the mantle superplume was substantiated. This thickening of the D" layer under Africa and the Pacific Ocean was identified based on seismic tomographic data as large low shear velocity provinces (LLSVPs) and interpreted as the accumulation of hot and heavy material, likely with a relatively high iron content [44, 47, 57].

The authors proposed a mantle flow tectonics model implying the following basic principles [33, 35].

(1) General mantle convection is the original driving force of tectonic processes. The additional effect of the rotating spheroid (rotational factor) on the motion of heated flows should not be ruled out, but it is not considered in our investigation.

(2) The ascending convection branch is formed by the general mantle superplumes of the Ethiopian–Afar and Central Pacific types.

(3) The superplumes generate sublithospheric upper mantle flows, which move the lithospheric plates due to a viscous friction. The flows are expressed as focused zones of reduced velocities of seismic waves propagating from the most intense seismic tomographic anomalies of superplumes. The position of spreading zones that developed in plate divergence areas varies under lateral increase of the plates. Subduction and collision zones are formed in the plate convergence area.

(4) Most subduction zones are fully or partially transformed into horizontal lenses (large mantle wedges) within the transitional mantle layer (~400–700 km). The subducting slabs submerging below [14] and the detached fragments of the large mantle wedges [59] constitute only part of the descending convection branch. The convection process also involves detachment and submergence of dense lower-lithospheric flows under cratons and intensive collision zones.

(5) In the period of widespread collision, it slows down the plate movement, and sublithospheric flows spread under the collision-adjacent areas. The flows get enriched in fluids by processing of the transitional mantle layer. The mantle activated in such a way partially replaces the mantle part of the lithosphere, and the flow fluids cause metamorphic transformations of the lithosphere and, as a consequence, decrease of its density. This process results in intensive activation of vertical motions at the second Pliocene-Quaternary stage of the Cenozoic mountain building.

(6) Analogs of the second stage fall on the end of the Hercynian (Artinskian Age) and Caledonian (Eifelian Age) tectonic cycles. These short stages were marked by reconstruction of the system of plate motions and, likely, of mantle flows.

In all the above-mentioned models, as in classical plate tectonics theory, a decisive role in the lithosphere displacement and deformation is played by the flow of the sublithospheric upper mantle material and related descending convection branches. Sorokhtin [31] gave reasons for the high velocity of the upper mantle flows under general mantle convection, based on the assumption of complete mantle circulation in the course of the tectonic cycle. At such high velocities, mineral transformations in the transitional mantle layer do not interrupt general mantle convection, resulting in rising or submergence of its boundaries only. Meanwhile, this assumption [31] remains hypothetical. According to all other models, the mantle flow velocities are also assumed to be much higher than those calculated from geological observation data on continental lithosphere deformations. The assumed velocities of mantle flows are related to the values of the calculated parameters based on assumptions and laboratory experiments, or they are a relatively indirect reflection on surface deformations.

In this paper, the rate of upper mantle flows and descending branches of general mantle convection has been determined by analysis of the geological and seismic tomographic data. The state of the upper mantle material, which is capable of ensuring the established flow velocities, is discussed. For the purpose of studying the mantle flows, global seismic tomographic data have been analyzed to construct a 3D model of seismic wave velocity variations in the Earth upon wave generation from natural sources such as earthquakes. This method is based on the selection of lateral velocity variations in the mantle with respect to the average values in such a way as to minimize the recorded discrepancies of the travel time obtained as the difference between the measured value and the theoretical value calculated by the radially symmetric velocity model. The degree of detail representation of the models for mantle velocity variations depends on the number of spherical harmonics used for spectral representation of the velocity variation field. At the end of the 2000s, 31st-order models were used to demonstrate the global pattern of variations. They are reviewed in [42]. The current regional models use higher-order harmonics [14] or parametrization values that are three to six times more detailed. Construction of regional models is effective in seismically active regions, e.g., in sub-Pacific subduction zones. As follows from comparison of the regional models with those by global network data, the latter yield a less accurate result, but they are qualitatively similar to the regional models [29]. Hence, global models of transverse wave velocity distribution V_S have been used to solve the problems of this paper.

The obtained variations δV_S with a negative sign are interpreted as a consequence of a heated and partially melted state of the Earth's interior, causing a decrease in local velocities. Variations δV_S with a positive sign are interpreted as cold substance of ancient cratons or as subducting slabs. This interpretation of δV, conventionally called "thermal," is generally accepted. Meanwhile, the upper mantle is characterized by considerable discrepancies in velocity variations obtained for different waves. Acceptable correlation coefficients begin at a depth greater than ~700 km. This indicates

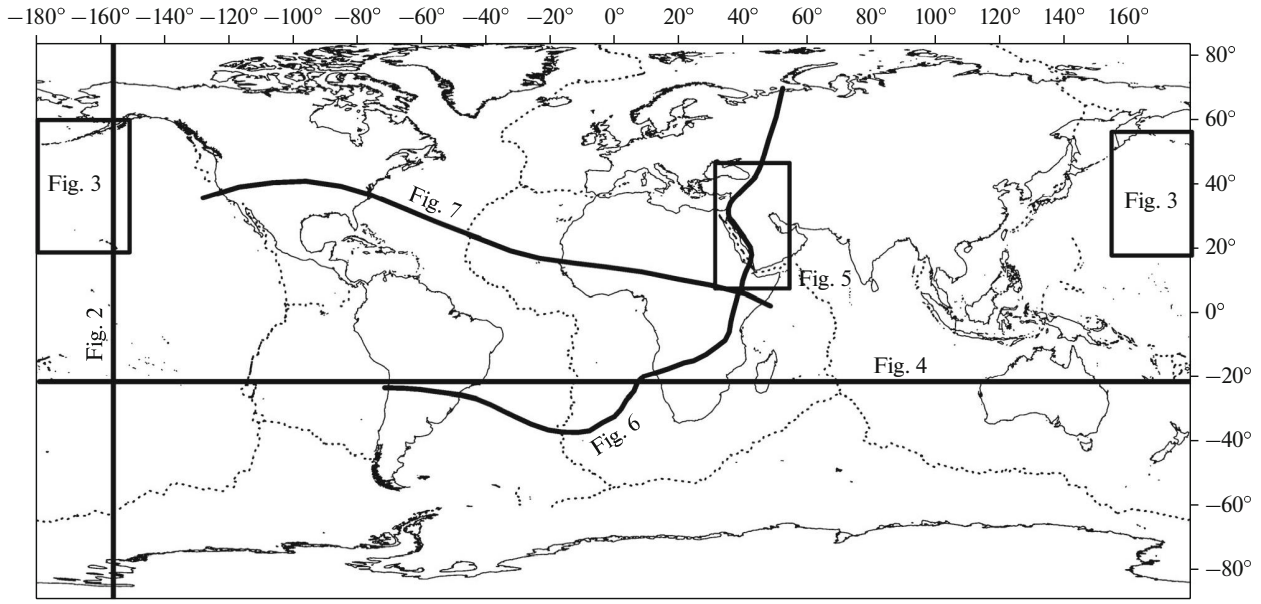

Fig. 1. Location of seismic tomographic sections shown in Figs. 2, 4, 6, 7 and maps shown in Figs. 3, 5. Location of mid-oceanic ridges is shown by dotted line.

the necessity to employ additional parameters to parametrize upper mantle flows.

RATES OF UPPER MANTLE LATERAL FLOWS

This paper reports two examples of calculating the rate of upper mantle flows based on manifestations of volcanism, the sources of which were, to one extent or another, fed by sublithospheric material: the Hawaii–Emperor Range in the Pacific Ocean and the region of Cenozoic volcanic eruptions stretching from Ethiopia to the Greater Caucasus. These examples characterize areas with different properties of the lithosphere, oceanic in the first case and continental in the second. Accordingly, the interpretation of volcanic manifestations in the context of assessing the sublithospheric flow velocity is different.

Hawaii–Emperor Range System

Interpretation of the Hawaii–Emperor Range system is based on the concept of a hot spot or a single plume [60, 72]. It is assumed that a hot ascending stream of mantle material "burns" the lithosphere and manifests itself on the Earth's surface as volcanic eruptions with geochemical signs of deep magma origin. Movement of the lithospheric plate over the stationary ascending flow is expressed as a chain of eruption traces whose age is consistently rejuvenated in one direction. The Hawaii–Emperor Range system is located at the northern end of the Central Pacific superplume (Figs. 1, 2). In addition to this system, the superplume controls other volcanic systems interpreted in the same way [27, 28]. The Hawaii–Emperor Range system differs from them in the unique duration of volcanic manifestations, at least from the Campanian (~76 Ma) to present time. The Pacific Plate changed the direction of motion ~47 Ma ago, thus changing the course of the volcanic chain (Fig. 3).

The plate motion rates have been calculated by the $^{40}Ar/^{39}Ar$ dates of volcanic rocks and their distance along the volcanic chain from the region of recent eruptions, Kilauea Island in the Hawaiian Archipelago (Table 1). Two data groups have been analyzed: the age of Pliocene–Quaternary eruptions in the islands of the Hawaiian Archipelago [63] and the age of the Campanian–Rupelian eruptions in the islands of the Emperor Range [48, 64, 67]. When analyzing the Pliocene–Quaternary data, we had no information what the eruption phase of a particular volcano is represented by the obtained eruption product date. Therefore, in the case of two or more dates from nearby points, preference has been given to the older date. The velocities of movement away from the Kilauea Volcano obtained for Mid–Late Quaternary rocks are considered overestimated, because the active Kilauea Volcano began to function long ago and the age difference between these rocks and the Kilauea Volcano is actually lower than it is when it is considered as recent. In the analysis of the Campanian–Paleogene volcanic rocks, preference has been given to the dates of the major eruption phase expressed as a shield volcano. The average velocity determined by the relative posi-

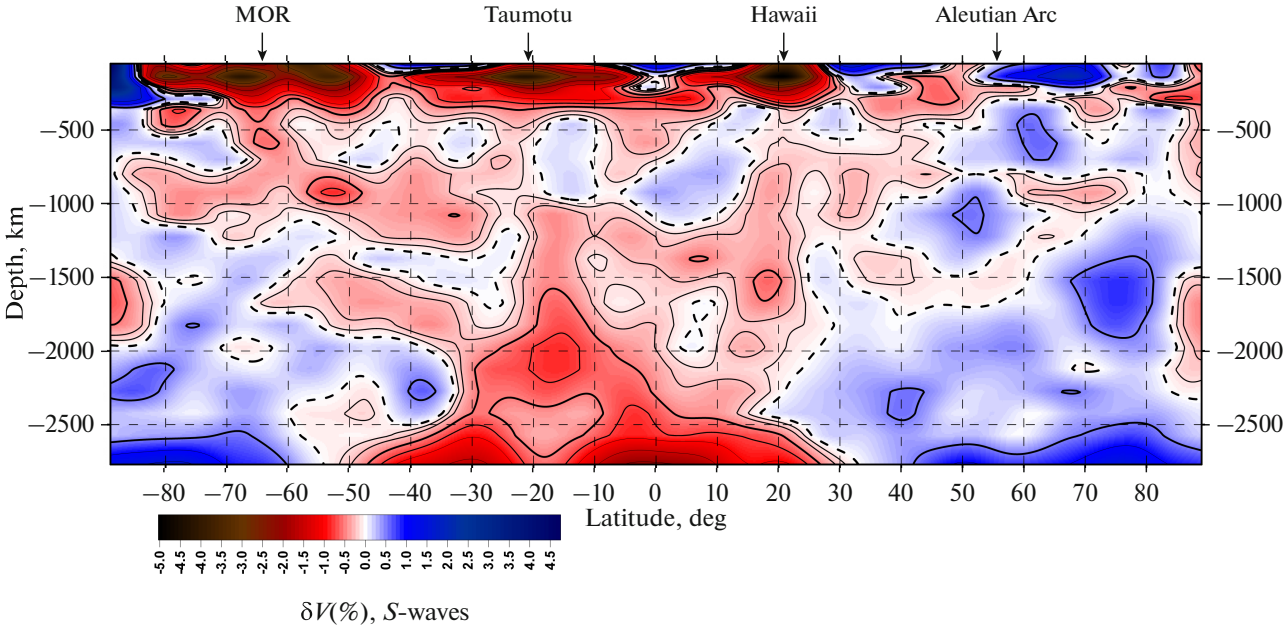

Fig. 2. Section δV of NGRAND seismic tomographic model [42, 54] based on *S*-waves from mantle roof to its base along Pacific Ocean superplume at longitude of Hawaii Islands. Profile position is shown in Fig. 1. Zero isoline is shown by dotted line.

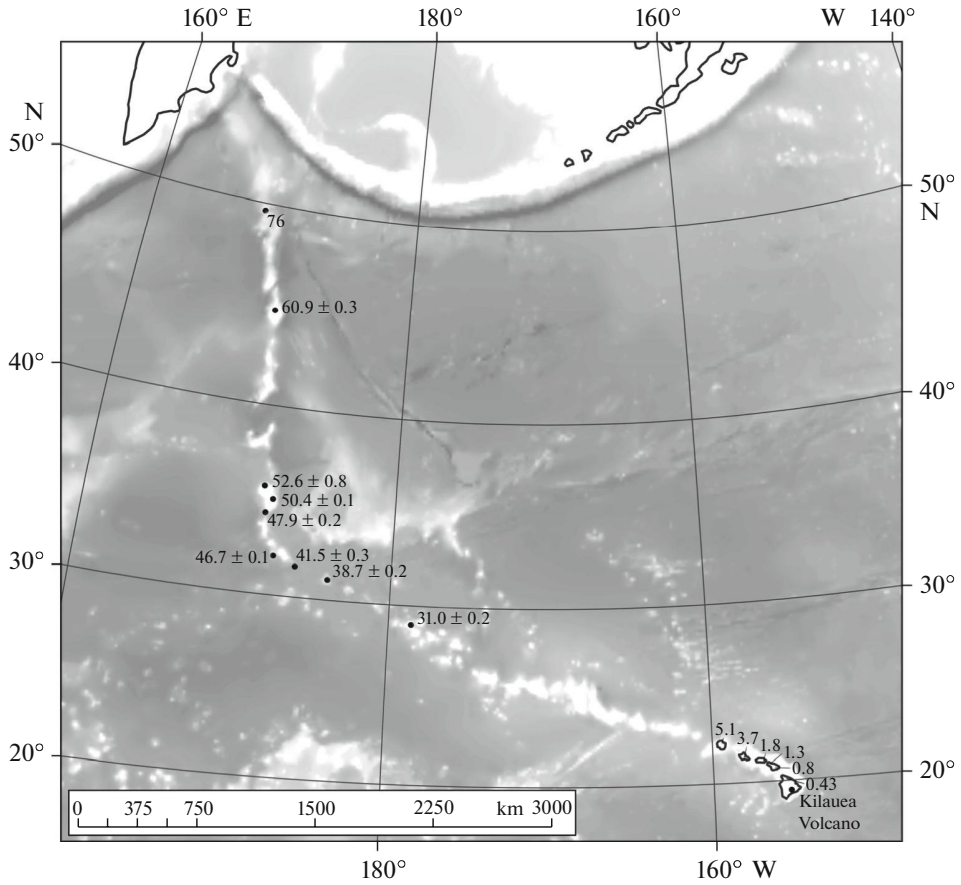

Fig. 3. System of volcanic islands of Hawaii–Emperor Range with $^{40}Ar/^{39}Ar$ dates of volcanic rocks, Ma (after data of [48, 63, 64, 67]).

Table 1. Removal rate of Pacific Plate to northwest relative to Kilauea Volcano (southeast of Hawaii Island)

No.	Volcano location	Distance to Kilauea Volcano, km	Eruption age, Ma	Removal rate, cm/yr
1	Hawaii, NW	65	0.43	15.0
2	Maui, east	115	0.8	14.4
3	Maui, west	140	1.3	10.8
4	Molokai	160	1.8	8.9
5	Oahu	230	3.7	6.2
6	Kauai	330	5.1	6.5
7	No name	2600	31.0 ± 0.2	8.4
8	Kolahan	3128	38.7 ± 0.2	8.1
9	Abbot	3280	41.5 ± 0.3	7.9
10	Diakakuji	3493	46.7 ± 0.1	7.5
11	Kimmei	3668	47.9 ± 0.2	7.7
12	Koko, south	3758	50.4 ± 0.1	7.5
13	Koko, north	3812	52.6 ± 0.8	7.3
14	Suiko	4860	60.9 ± 0.3	8.0
15	Detroit	5600	76	7.4

Plate movement direction changed between 10 and 11 ~47 Ma ago.

tion of the earliest dated eruptions reaches ~7.4 cm/yr. This rate changed in the course of time. It increased up to ~12 cm/yr in the period from the Middle Paleocene to the Early Eocene and fell to ~4.5–6.5 cm/yr in other Paleogene epochs.

As follows from the analysis of the seismic tomographic data, the extended meridionally elongated Central Pacific superplume only locally appears at the ocean bottom as single volcanic highlands or volcanic chains similar to the Hawaii–Emperor Range system, but usually shorter. The ascending superplume groundmass was transformed above the transitional mantle layer into lateral flows extending both westwards and eastwards. The eastward flows reached the East Pacific uplift and extended, submerging, to the boundary with the thickened South American lithosphere (Fig. 4). It is assumed that these flows led to the

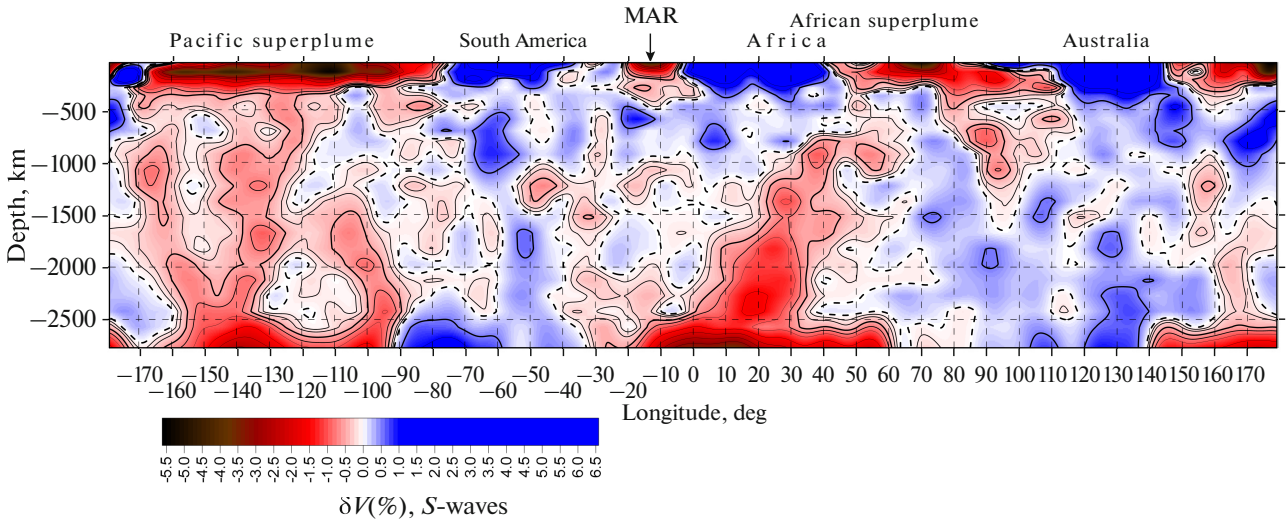

Fig. 4. Section δ*V* of NGRAND seismic tomographic model [42, 54] based on *S*-waves from mantle roof to its base along 22° S. Profile position is shown in Fig. 1. Zero isoline is shown by dotted line.

formation of the East Pacific uplift and the corresponding spreading zone and to the eastward movement of the Nazca Plate. In addition, flatten –cellular upper mantle convection resulting in northwestward movement of the Pacific Plate appears west of the spreading zone [9, 22, 35, 38]. The estimated average travel rates of the plate are the minimum rates of sublithospheric flows that move the Pacific Plate. According to calculations by V.P. Trubitsyn and M.N. Evseev [70], the interruptive expression of the ascending mantle flow as the chain of volcanic islands in the Hawaii–Emperor Range system is due to autooscillatory material uplifted from depth, which ensured the impulse nature of material supply to the surface in million-year intervals.

Ethiopia–Arabian Plate–Caucasus System

The East African–Transcaucasian belt of the Cenozoic volcanism extends from the East Africa rifts to the Greater Caucasus [41]. The investigation objective is targeted on its part covering the Ethiopian Highlands, the west of the Arabian Plate and the adjacent Arabian–Caucasian segment of the Alpine–Himalayan orogenic belt. If we exclude from consideration the Eocene and more rare Oligocene volcanic rocks and granitoid intrusions related to the closure of the residual back-arc Neotetis basins, as well as the Late Miocene trachyte extrusions of the Caucasian Mineral Waters region likely reflecting the local collision interactions, other manifestations of volcanism in the studied region are characterized by a definite uniformity. These are subaerial manifestations of volcanism, where a position and a functioning time of the eruption centers are controlled by tectonic settings [24, 69].

The magmatic foci of the volcanoes in the discussed region, often developed for a long time, show signs of feeding from the deep mantle sources. The Ethiopian Highlands eruptions had a basic composition, occasionally, with an increased alkalinity. The eruptions occurred over the top of the Ethiopian–Afar superplume and are considered to be manifestations of it [49]. The volcanic rocks of more northern regions are situated above the sublithospheric upper mantle flow extending from the superplume [29]. All researchers agree that basalts of the western Arabian Plate are of mantle origin. Their common source is confirmed by the homogeneity of basalts by the Sr–Nd isotope ratios [65]. In opinion of M. Lustrino and E.V. Sharkov [58], regional primitive magmas could be generated by spinel/garnet-bearing lherzolite sources at a depth of up to 90 km, that is to say, at the bottom of the lithosphere. They were related to local decompression areas likely caused by sublithospheric flows. This conclusion follows from the fact that the sources moved together with the Arabian Plate, and their long, occasionally up to a few tens of millions of years, functioning required a deep material–energy supply [69].

The eruption products in the Arabian–Caucasian segment of the Alpine–Himalayan belt belong to the calc–alkaline range and are occasionally distinguished by a higher alkalinity along the periphery of the volcanic area. According to the thermodynamic calculation data obtained by N.V. Koronovskii and L.I. Demina [18, 19], correlated with the geochemical and petrological investigation data on the Late Cenozoic volcanic rocks, the magma was generated in the southern Armenian Highland at a pressure of $P = 1.1–1.2$ GPa, characteristic of the top of the mantle, while in the northern highland and in the Greater Caucasus, the magma was generated at $P = 0.95–1.05$ GPa, $T = 850°–1100°$ at a depth of 35–40 km. In the northern Armenian Highland, it is the lowest part of the Earth's crust, close to its base, and in the Greater Caucasus, it is the lower crustal layer [20]. The depth of felsic magma generation in the Elbrus Region is estimated at 17–25 km. Felsic magmas are assumed to be related to an intermediate magmatic chamber. In addition, rocks with a reduced seismic wave velocity and an increased electrical conductivity, identified as the major magmatic focus, were found under Elbrus at a depth of 35–50 km [25]. The data on the Sr–Nd–O isotopic ratios in the regional volcanic rocks, as well as the high $^3He/^4He$ ratios in the Elbrus and Kazbek sources, are evidence for the mantle material supply to the magmatic foci [6, 15, 26]. Basalts of the Armenian Highland are somewhat similar to basalts of ensialic island arcs and active continental margins [17]. The seismic wave velocity decreases by 1.5% in the subcrustal mantle of the Elbrus Region [23]. Taking into consideration these data, Koronovskii and Demina [19] proposed a model for regional Late Cenozoic magma generation, according to which magma foci at the bottom of the Earth's crust and in the uppermost mantle appeared with involvement of the heat and mass transfer products from deeper levels of the mantle, that is to say, they had feeding sources in its sublithospheric part.

A.V. Ershov and A.M. Nikishin [12] noted a consistent northward rejuvenation of regional volcanic rocks and suggested it was related to possible movement of the sublithospheric flow front from the Ethiopian–Afar superplume. The existence of such a flow was validated by the discovery of the low-velocity sublithospheric mantle [13, 46]. Later, new datings of manifestations of volcanism made it possible to specify their northward rejuvenation [69]. The presence of the sublithospheric flow traced from the Ethiopian–Afar superplume to the Greater Caucasus was confirmed by analysis of global seismic tomographic data [29].

The age of the earliest manifestations of volcanism over the Ethiopian–Afar superplume and at different distances from it northwards should be known in order to determine the removal rate of the sublithospheric flow. The obtained data are shown in Fig. 5. The age of the earliest manifestations of volcanism within the Ethiopian volcanic highland was estimated at ~55 Ma [16]; on the northeastern shore of the Red Sea in Saudi

Table 2. Removal rates of upper mantle flow from Ethiopian–Afar superplume to north

No.	Dating point	Age, Ma	Distance, km	Trend distance, km	Rate along trend, cm/yr	
1	Ethiopian Highlands	55	0			
2	NE shore of Red Sea	32	1800 (1–2)	1740	7.8 (1–2)	
3	Palmyrides, Ed Dau	25	1450 (2–3)	1400	20.0 (2–3)	14.0 (2–4)
4	Karamanmarash	20	410 (3–4)	400	8.0 (3–4)	
5	Euphrates right shore NW of Mt. Malatya	17	185 (4–5)	110	3.7 (4–5)	4.1 (4–7)
6	Akhalkalaki	8	519 (5–6)	400	4.4 (5–6)	
7	Elbrus	2.8	218 (6–7)	200	4.0 (6–7)	

Numbers of points between which flow distances and velocities have been determined are shown in brackets.

Arabia, ~ 32 Ma [45]. Further north, reliable dates for the earliest manifestations of volcanism were obtained in the Ed Dau Basin in Palmyrides, Syria, ~25 Ma [40], and at the northern edge of the Arabian Plate southeast of Karamanmarash in southern Turkey, ~20 Ma [68]. We have discovered three basaltic covers ~17 Ma in age on the right bank of the Euphrates River northwest of Malatya among Miocene terrigenous rocks. The following northwards date of ~8 Ma was obtained in the northwestern Javakheti Highlands near Akhalkalaki in Georgia [21]. Lastly, the age of the oldest volcanic structures in the Elbrus Region was estimated at ~2.8 Ma [19].

In order to estimate the travel rate of the sublithospheric flow in the entire region both from the Early Eocene to the Late Pliocene and in separate time intervals, it is also necessary to estimate the distances this flow travels during this time. It is evident that these estimates should be obtained not by distances between the age determination points of volcanic rocks, but by projections of these distances on the general trend of flow travel identified by the concentration of eruption centers and volcanic rocks close to the meridian. Calculations have yielded the following results (Table 2). The average flow rate determined by the distance along the trend from the Lower Eocene outcrops in the Ethiopian Highlands to Elbrus (~4250 km) and the above-mentioned extreme values of the age of volcanic rocks is ~8.1 cm/yr. In the segment between the above-mentioned Lower Eocene outcrops and the northeastern side of the Red Sea (distance ~1740 km, age difference ~23 Ma), the obtained rate is close to the average value, ~7.8 cm/yr. Under the Arabian Plate, the flow rate increases to 13–14 cm/yr, and its values determined by distances between points located in different parts of the plate differ drastically, likely due to errors in the estimated age of rocks or the uncertain location of basaltic eruption centers. The flow rate decreases to 3.7–4.4 cm/yr and averages 4.1 cm/yr under the Arabian–Caucasian segment of the orogenic belt and near its southern boundary (the South Taurus overthrust).

The two given rate estimates of sublithospheric flows in the upper mantle are similar in magnitude, while representing different structural conditions. Due to the fact that under interaction with the neighboring plates the Pacific Plate could be somewhat slow relative to the sublithospheric flow moving it, the average flow rate likely exceeded the established average plate drift rate of ~7.4 cm/yr and reached ~8 cm/yr, thus making the obtained estimates even more similar. In the Arabian–Caucasian Region, the flow rate is many times greater than the drift rate of the Arabian Plate and orogenic belt deformation, based on GPS measurement results, paleomagnetic data, estimated rates of lateral displacements at the plate boundaries, and deformation rates in the belt [5, 24, 34].

HIGH-VELOCITY MANTLE VOLUMES AS A REFLECTION OF THE DESCENDING GENERAL MANTLE CONVECTION BRANCH

As follows from the seismic tomographic mantle profiles crossing both oceanic and continental regions, the upper mantle flows expressed as lower seismic wave velocities, although growing thinner, are not interrupted under continents [29]. W. Fjeldskaar [50] estimated the thickness of the asthenosphere under Fennoscandia at 25–100 km. In the European Geotraverse (EGT), the thickness of the lithosphere under Fennoscandia is ~220 km where the asthenosphere is ~80 km thick [43]. According to [55], the thickness of the lithosphere under continents does not exceed 200–250 km, and the seismic interpretations indicating its greater thickness do not take into account anisotropy of the asthenosphere.

The mantle profiles compiled by analysis of global seismic tomographic data [42, 54] also cross both oceanic and continental regions (Figs. 4, 6, 7). These profiles show thickening of the low-velocity volumes of the D" layer under Africa and the Pacific Ocean, generating the Ethiopian–Afar and Pacific superplumes upwards. In addition, the relatively high-velocity

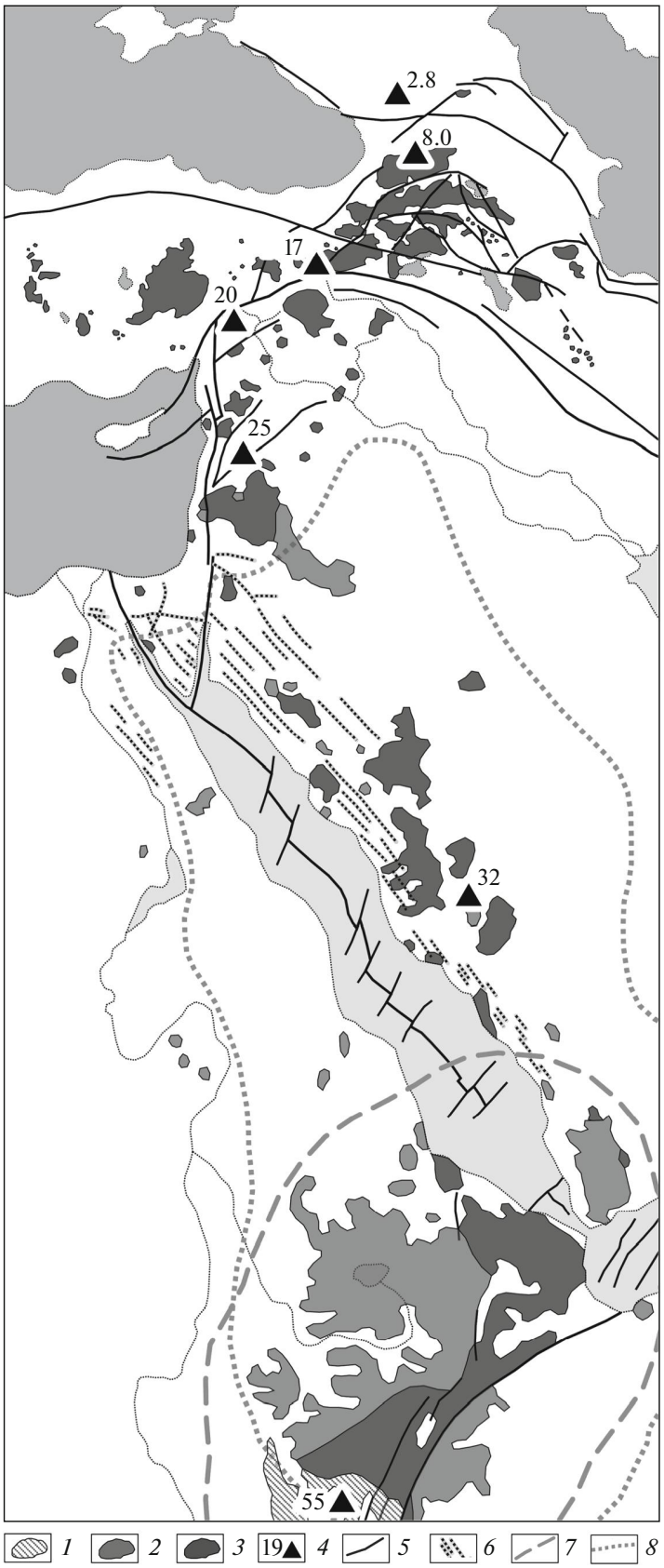
2.8
8.0
17
20
25
32
55
1
2
3
19
4
5
6
7
8

Fig. 5. Radioisotope dates of volcanic manifestations at newest development stage of Arabian–Caucasian Region, marking distribution of sublithospheric upper mantle flow [after data of 16, 19, 21, 40, 45, 68]. Arbitrary notes: (*1–3*) Volcanic rocks: (*1*) Eocene; (*2*) Oligocene, Early and Middle Miocene; (*3*) Late Miocene, Pliocene, and Quaternary; (*4*) dating points of volcanic manifestations that mark motion of sublithospheric stream (numerals near sign indicate age, Ma); (*5*) major Late Cenozoic faults; (*6*) dike belts; (*7*) Ethiopian–Afar superplume contour; (*8*) African–Arabian Uplift.

mantle materials are distinguished under a thickened continental lithosphere (Figs. 4, 6). These fragmented volumes extend to the lower mantle, gradually losing their individual nature with depth. They are characterized by more significant deviations from the average statistical values than those with near-zero values or anomalies of less than 1% between strong focused "hot" anomalies of more than –1%. Such high-velocity volumes on both coasts of the Atlantic Ocean can be clearly traced to a depth of ~1000 km and less certainly to 2000–2200 km. In both coasts, the band with these volumes is inclined towards the Mid-Atlantic Ridge so that at a depth of 2000–2200 km, this volume under Africa is located ~10°–20° westwards relative to its position in the upper mantle, and under South America, respectively, 20°–30° eastwards. Similar high-velocity volumes under the North American Platform also form a band inclined towards the Atlantic Ocean and shifted 30°–35° eastwards in the lower mantle (Fig. 7).

According to the mantle flow tectonics model presented by the authors, the high-velocity mantle volumes consist of the dense lowest parts of the thickened continental lithosphere detached by upper mantle flows; under South America, they also include fragments of the subducted Pacific Ocean slab. The long-term submergence of detached fragments was simultaneous with opening of the Atlantic Ocean. Therefore, the fragments that began to submerge earlier and, correspondingly, reached greater depths are now closer to the Mid-Atlantic Ridge than the fragments generated in the course of later detachment. If we add the mutual approach of high-velocity volumes on the opposite sides of the Atlantic Ocean towards its expansion, then the approach will be 45°–50°, which roughly coincide with the magnitude of the Atlantic Ocean opening. Consequently, submergence of the high-velocity volumes began no later than opening of the Atlantic Ocean. Taking into account the fact that the incline of the axis and the boundaries of these volumes does not show changes with depth, it can be assumed that the mantle submergence time and the Atlantic opening time are approximately the same. It is established that the Atlantic Ocean began to form in the system of grabens that developed in the continent of Gondwana in the Late Permian. In the Early Jurassic, their extension in the Central Atlantic turned into ocean spreading. Hence, the detached high-velocity volumes submerged to a depth of 2000–2200 km in the last ~200 Ma. If we take into account the fact that they were originally located under thickened layers of the continental lithosphere at a depth of ~200 km, then the average submergence rate reached 0.9–1.0 cm/yr. This value is almost an

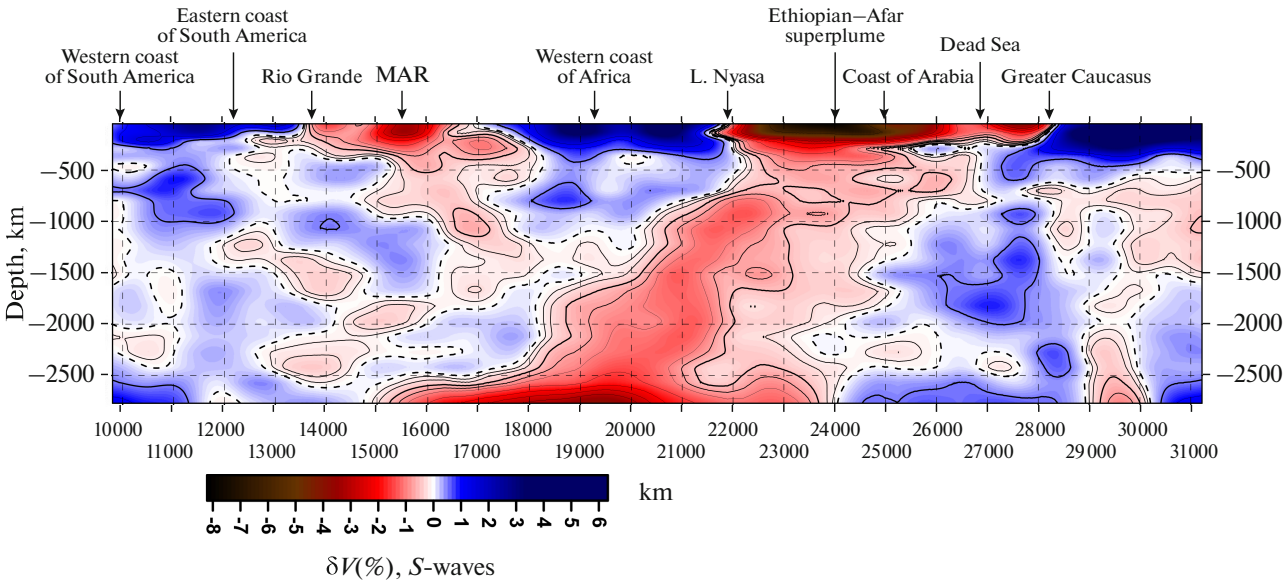

Fig. 6. Section δV of NGRAND seismic tomographic model [42, 54] based on *S*-waves from mantle roof to its base from western coast of South America across Atlantic Ocean, Africa, and Arabia to East European Platform. Profile position is shown in Fig. 1. Zero isoline is shown by dotted line.

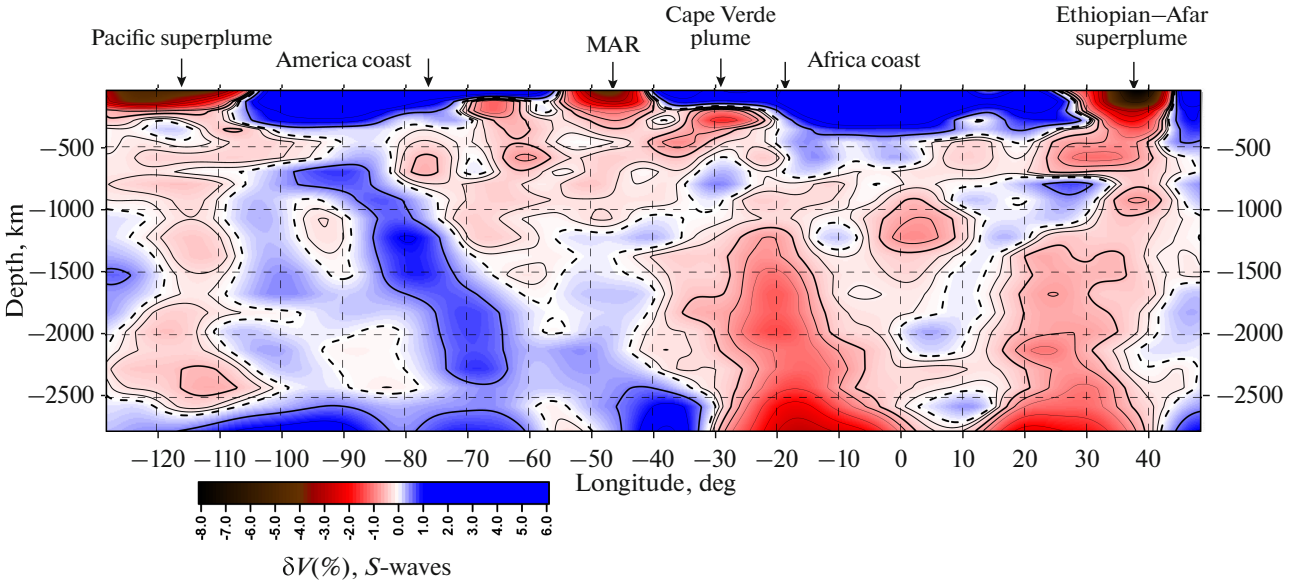

Fig. 7. Section δV of NGRAND seismic tomographic model [42, 54] based on *S*-waves from mantle roof to its base from east of Pacific Ocean through North America, Atlantic Region, and Central Africa. Profile position is shown in Fig. 1. Contours are spaced at 0.5%. Zero isoline is shown with a dotted line.

order of magnitude lower than the travel rate of the upper mantle flows determined above.

The area of relatively high-velocity mantle volumes beginning under the Scythian Plate and traced to a depth of ~ 2000 km was identified in the seismic tomographic profile covering the Ethiopian–Afar superplume, the Arabian–Caucasian segment of the Alpine–Himalayan belt and the Eastern European Platform [29]. Its lower part is located ~1000–1500 km farther south than its upper part. A similar slope was revealed for a high-velocity volume starting under the collision-thickened layer of the Himalayan lithosphere and a possible slab of the Neotethys oceanic lithosphere (Indus–Zangpo zone). This high-velocity region can be traced to a depth of ~2200 km, shifting southwards to a distance of up to 1500 km. In both cases, the slope of the high-velocity region is indicative of the relative motion of the continental lithosphere in the northern bearing lines; in the latter case, the submergence process affected the lithosphere fragments detached in the course of the Late Mesozoic–Cenozoic subduction and subsequent collision.

DISCUSSION

According to the recent ideas of mantle properties, material flows in the mantle mainly by the diffusion creep (plasticity) mechanism, to which Newtonian fluid properties are applicable. In the top of the upper mantle and, likely, in the submerged volumes of the lithospheric substance below this level, flow can also be subject to the dislocation creep (quasi-plasticity) mechanism. The viscosity of the medium based on temperature and pressure is of critical importance in calculating the flow parameters by the diffusion creep mechanism. If lithostatic pressure depends on the load of the overlying rocks, and hydrostatic pressure—on the weight of the fluid column, then the total temperature change with depth is affected by the ascending and descending currents. The dislocation creep calculations require, in addition, the tectonic stress data.

The existing estimates of the effective mantle viscosity are based on data on Holocene vertical movements related to deglaciation unloading of the ancient cratons. Artyushkov [2] used these data to estimate the viscosity of the asthenosphere at 10^{19}–10^{20} Pa s. The estimate given in [50] reaches 7×10^{19} Pa s for Fennoscandia. The viscosity of the entire mantle was modeled from data on ice unloading [61]. According to this model, the viscosity in the top of the upper mantle is within 10^{19}–10^{20} Pa s. It increases to ~10^{21} Pa s to the bottom of the transitional layer, rises to ~10^{22} Pa s at the boundary of the lower mantle, and remains almost unchanged to the boundaries of the thickened D" layer with lower velocities of transverse waves, where it decreases to 10^{19}–10^{20} Pa s. The obtained values are much lower than the viscosity of the lithosphere, which is estimated at 10^{21}–10^{26} Pa s for different tectonic provinces beyond the local thermal overflow and strain concentration zones [3, 39, 66]. This rules out the effect of the specific features of the tectonic flow in the mantle on the lithosphere. Convective flows in the sublithospheric mantle cause lithosphere deformations and displacements directly or indirectly by the dislocation creep and brittle crushing mechanism.

Trubitsyn [37, 38] used the values obtained in laboratory experiments with olivine [56] in numerical modeling of the viscosity distribution under general mantle convection. The calculation formula includes the constant parameters E_0 (activation energy) and V_0 (activation volume). Application of the experimental data to solving the convection equations shows a higher viscosity in the lower mantle up to 10^{24}–10^{25}, making convection ineffective in the lower mantle. This impels to look for other lower mantle deformation sources and mechanisms [62]. In order to achieve consistency with the data of [61], Trubitsyn made the parameter V_0 twice as low. Meanwhile, the flow rate in the upper mantle (~10 cm/yr), similar to our geological data interpretation results, has been obtained in modeling at a viscosity value of ~10^{18} Pa s, which is one to two orders of magnitude lower than the values resulting from the deglaciation rebound data.

The reported values and relationships are indicative of considerable discrepancies in the estimated parameters of mantle flows. Our new data on the rates of the lateral upper mantle and descending flows of the mantle material introduce certain limitations in the numerical simulation of mantle flows. Our estimated flow rates in the upper mantle and descending flows differ by almost an order of magnitude. As for the ascending flows in the superplumes, we can state the following. Investigating the correlation of seismic flow parameters in the Kurils–Kamchatka and Pamir–Hindukush mantle seismic focal zones, G.A. Vostrikov [7, 8] did not reveal a numerical dependence of seismic wave velocity on the effective viscosity, but he proved that higher velocities generally correspond to increased viscosity of the medium. If these relations are applied to ascending mantle streams, despite the fact that the material likely flows there by the diffusion creep mechanism rather than by the dislocation creep as in the seismic focal zones, we can expect higher flow rates in these flows than in the surrounding mantle. It is possible that they are similar, on average, to rates of the upper mantle flows.

The discrepancies in the estimated flow viscosity and velocity in the sublithospheric upper mantle can be related to the expected specific features of its structure. Such definitions as a brecciated or granulated medium can likely be applicable to it. The asthenosphere is assumed to be composed of hard fragments from individual grains to large blocks separated by thin substance films occupying a small percentage of the total volume; the substance is close to the melting state and possibly occasionally saturated with fluids, with which the asthenospheric streams enriched during transport, by processing of the transition layer material [35]. The presence of the interblock and intergranular matrix with a dramatically reduced viscosity permits the general deformation and high-rate flow of relatively hard fragments.

CONCLUSIONS

This paper reports geological data on the travel rates of upper mantle sublithospheric flows in the Hawaii–Emperor Range and the Ethiopian–Arabia–Caucasus systems. In the first case, the estimation is based on motion of the asthenospheric flow and the Pacific Plate moved by it over the northern branch of the Central Pacific plume. Magmatic plume products penetrated through the stream and the plate and manifested themselves on the Earth's surface as volcanic eruptions. The travel rate has been determined by the position of variably aged volcanoes relative to the active Kilauea Volcano, which is located above the plume branch. The age of the recorded volcanoes is estimated at 76 Ma–to present time. The travel rate varied in different epochs from ~12 to 5 cm/yr, 7.4 cm/yr on average. Because the sublithospheric flow could move faster than the plate, its travel rate was likely close to 8 cm/yr.

The travel rate of the Ethiopia–Arabia–Caucasus asthenospheric flow has been calculated in a different way. The stream spread in the northern bearing lines from the Ethiopian–Afar superplume, and the onset of volcanic eruptions at each flow path point indicated that the flow reached this point. Volcanic eruptions with the age of 55–2.8 Ma have been recorded. The travel rates varied in different epochs from 12 to 4 cm/yr, and they were higher under the Arabian Plate than under the Alpine–Himalayan collision belt. The average rate was 8.1 cm/yr.

Analysis of global seismic tomographic data has made it possible to identify the mantle rock volumes under continents, characterized by a higher velocity of seismic waves propagating to the lower mantle, where they gradually lose their individual features. It is suggested that these volumes are related to submergence of the detached fragments of the thickened lithosphere, and they represent the descending branch of general mantle convection. Under South America, high-velocity volumes can also include subducted near-Pacific slabs. On both sides of the Atlantic Ocean, such volumes are inclined towards the Mid-Ocean Ridge. This means that the earlier the volume began to submerge, the closer it is to the ridge. Deviation of the submergence axis from the vertical is related to opening of the ocean, and the total of deviations on both sides of the ocean coincide with the total magnitude of its opening. The submergence of the identified high-velocity volumes started simultaneously with the beginning of opening of the ocean, making it possible to determine their submergence rate: 0.9–1.0 cm/yr, which is almost an order of magnitude lower than the determined flow rates in the upper mantle and is likely considerably lower than the rate of the ascending mantle flows in superplumes.

The estimated rates of mantle flows make it possible to clarify the deformation properties of the mantle

and to regulate the numerical models of mantle convection.

ACKNOWLEDGMENTS

The studies were financed by the Russian Science Foundation (project no. 17-17-01073).

REFERENCES

1. E. V. Artyushkov, "Gravitational convection in the Earth's interior," Izv. Akad. Nauk SSSR. Fiz. Zemli, No. 9, 3–18 (1968).
2. E. V. Artyushkov, *Geodynamics* (Nauka, Moscow, 1979) [in Russian].
3. E. V. Artyushkov, *Physical Tectonics* (Nauka, Moscow, 1993) [in Russian].
4. E. V. Artyushkov, "Neotectonic crustal uplifts as a consequence of mantle fluid infiltration into the lithosphere," Russ. Geol. Geophys. **53**, 566–582 (2012).
5. M. L. Bazhenov and V. S. Burtman, *Structural Arcs of the Alpine Belt: Carpathians–Caucasus–Pamir* (Nauka, Moscow, 1990) [in Russian].
6. S. N. Bubnov, Yu. V. Gol'tsman, and B. G. Pokrovskii, "Sr, Nd, and O isotopic systems as indicators of the origin and evolution of the primary melts for contemporary lavas in the Elbrus volcanic area, Greater Caucasus," *XIV Symposium on Isotope Geochemistry, Moscow, Russia, 1995* (GEOKhI, Moscow, 1995), pp. 28–29.
7. G. A. Vostrikov, "Deep regional structure and geodynamic characteristics of the Kuril-Kamchatka focal zone," in *Neotectonics and Contemporary Geodynamics of the Mobile Belts* (Nauka, Moscow, 1988), pp. 116–135.
8. G. A. Vostrikov, "Nonuniformity of seismic flow process in the Pamir–Hindu Kush hypocentral zone of intermediate earthquakes," in *Neotectonics and Contemporary Geodynamics of the Mobile Belts* (Nauka, Moscow, 1988), pp. 219–233.
9. N. L. Dobretsov, A. G. Kirdyashkin, and A. A. Kirdyashkin, *Deep Geodyanamics* (Sib. Otd. Ross. Akad. Nauk, Novosibirsk, 2001) [in Russian].
10. A. A. Kirdyashkin, N. L. Dobretsov, and A. G. Kirdyashkin, "Thermochemical plumes," Russ. Geol. Geophys. **45**, 1005–1024 (2004).
11. N. L. Dobretsov and A. F. Shatskiy, "Deep carbon cycle and geodynamics: The role of the core and carbonatic melts in the lower mantle," Russ. Geol. Geophys. **53**, 1117–1132 (2012).
12. A. V. Ershov and A. M. Nikishin, "Recent geodynamics of the Caucasus–Arabia–East Africa region," Geotectonics **38**, 123–136 (2004).
13. A. V. Ershov, A. M. Nikishin, M.-F. Brunet, and W. Spakman, "Late Cenozoic geodynamics of the Caucasian region: Numerical modeling data and seismic tomography," in *Tectonics of the Neogean: General and Regional Aspects* (GEOS, Moscow, 2001), Vol. 2, pp. 230–235.
14. D. Zhao, F. Pirajno, N. L. Dobretsov, and L. Liu, "Mantle structure and dynamics under East Russia and adjacent regions," Russ. Geol. Geophys. **51**, 925–938 (2010).
15. D. A. Ivanov, S. N. Bubnov, V. M. Volkova, Yu. V. Gol'tsman, D. Z. Zhuravlev, and E. D. Bairova, "Isotope composition of Sr and Nd in Quaternary lavas of the Greater Caucasus with respect to the problem of their petrogenesis," Geokhimiya, No. 3, 343–353 (1993).
16. V. G. Kaz'min, *Rift Structures of East Africa: Continental Breakup and Origination of the Ocean* (Nauka, Moscow, 1987) [in Russian].
17. Yu. V. Karyakin, *Geodynamics of the Formation of Volcanic Complexes in the Lesser Caucasus* (Nauka, Moscow, 1989) [in Russian].
18. N. V. Koronovskii and L. I. Demina, "Collision stage of the evolution of the Caucasian sector of the Apline Foldbelt: Geodynamics and magmatism," Geotectonics **33**, 102–118 (1999).
19. N. V. Koronovskii and L. I. Demina, "Late Cenozoic volcanism of the Greater Caucasus," in *Greater Caucasus in the Apline Epoch* (GEOS, Moscow, 2007), pp. 251–284.
20. G. V. Krasnopevtseva, *Deep Structure of the Caucasian Seismoactive Region* (Nauka, Moscow, 1984) [in Russian].
21. V. A. Lebedev, I. V., Chernyshev, M. M. Arakelyants, Yu. V. Gol'tsman, O. Z. Dudauri, and G. T. Vashakidze, "Geochronology of the Neogene–Quaternary dacitic volcanism in the northwestern Lesser Caucasus (Georgia)," Stratigr. Geol. Correl. **12**, 85–101 (2004).
22. L. I. Lobkovsky, "Deformable plate tectonics and regional geodynamic model of the Arctic region and Northeastern Asia," Russ. Geol. Geophys. **57**, 371–386 (2016).
23. E. E. Milanovskii, L. M. Rastsvetaev, S. U. Kukhmazov, A. S. Birman, N. N. Kurdin, and V. G. Simako, "Recent geodynamics of the Elbrus–Mineral'nye Vody region, Northern Caucasus," in *Geodynamics of the Caucasus* (Nauka, Moscow, 1989), pp. 99–105.
24. *Neotectonics, Contemporary Geodynamics, and Seismic Hazard of Syria*, Ed. by V. G. Trifonov (GEOS, Moscow, 2012) [in Russian].
25. *Recent and Contemporary Volcanism in Russia*, Ed. by N. P. Laverov (Nauka, Moscow, 2005) [in Russian].
26. B. G. Polyak, I. L. Kamenskii, E. M. Prasolov, A. L. Cheshko, L. N. Barabanov, and G. I. Buachidze, "Helium isotopes in gases of the Norther Caucasus: Implications for heat and mass influx from the mantle," Geochem. Int. **36**, 329–342 (1998).
27. V. N. Puchkov, "The controversy over plumes: Who is actually right?," Geotectonics **43**, 1–17 (2009).
28. V. N. Puchkov, "Relationship between plume and plate tectonics," Geotectonics **50**, 425–438 (2016).
29. S. Yu. Sokolov and V. G. Trifonov, "Role of the asthenosphere in transfer and deformation of the lithosphere: The Ethiopian-Afar superplume and the Alpine-Himalayan Belt," Geotectonics **46**, 171–184 (2012).
30. O. G. Sorokhtin, *Global Evolution of the Earth* (Nauka, Moscow, 1974) [in Russian].

31. O. G. Sorokhtin, *Life of the Earth* (NITs Regulyarnaya i Khaoticheskaya Dinamika, Moscow, 2007) [in Russian].
32. *Tectonic Layering of the Lithosphere and Regional Geological Studies*, Ed. by Yu. M. Pushcharovskii and V. G. Trifonov (Nauka, Moscow, 1990) [in Russian].
33. V. G. Trifonov, "Collision and mountain building," Geotectonics **50**, 1–20 (2016).
34. V. G. Trifonov, O. V. Soboleva, R. V. Trifonov, and G. A. Vostrikov, *Contemporary Geodynamics of the Alpine–Himalayan Collisional Belt* (GEOS, Moscow, 2002) [in Russian].
35. V. G. Trifonov and S. Yu. Sokolov, "Toward postplate tectonics," Her. Russ. Acad. Sci. **85**, 331–341 (2015).
36. V. P. Trubitsyn, "The tectonics of floating continents" Her. Russ. Acad. Sci. **75**, 7–18 (2005).
37. V. P. Trubitsyn, "Viscosity distribution in the mantle convection models," Izv., Phys. Solid Earth **52**, 627–636 (2016).
38. V. P. Trubitsyn and A. P. Trubityn, "Numerical model for the generation of the ensemble of lithospheric plates and their penetration through the 660-km boundary," Izv., Phys. Solid Earth **50**, 853–864 (2014).
39. V. E. Khain and M. G. Lomize, *Geotectonics and Fundamentals of Geodynamics* (Mosk. Gos. Univ., Moscow, 1995) [in Russian].
40. E. V. Sharkov, I. V. Chernyshev, E. V. Devyatkin, A. E. Dodonov, V. V. Ivanenko, M. I. Karpenko, Yu. G. Leonov, V. M. Novikov, S. Hanna, and K. Khatib, "Geochronology of Late Cenozoic basalts in Western Syria," Petrology **2**, 385–394 (1994).
41. V. V. Yarmolyuk, O. A. Bogatikov, and V. I. Kovalenko, "Late Cenozoic transcontinental structures and magmatism of the Earth's Euro-African segment and geodynamics of its formation," Dokl. Earth Sci. **395**, 183–186 (2004).
42. T. W. Becker and L. Boschi, "A comparison of tomographic and geodynamic mantle models," Geochem. Geophys. Geosyst. **3**, (2002). doi 10.1029/2001GC000168
43. D. J. Blundell, "The legacy of the European Geotraverse," Tectonophysics **314**, 7–16 (1999).
44. A. L. Bull, A. K. McNamara, and J. Ritsema, "Synthetic tomography of plume clusters and thermochemical piles," Earth Planet. Sci. Lett. **278**, 152–162 (2009).
45. V. E. Camp and M. J. Roobol, "Upwelling asthenosphere beneath western Arabia and its regional implication," J. Geophys. Res.: Solid Earth **97**, 15255–15271 (1992).
46. E. Debayle, J.-J. Leveque, and M. Cara, "Seismic evidence for a deeply rooted low-velocity anomaly in the upper mantle beneath the northeastern Afro/Arabian continent," Earth Planet. Sci. Lett. **193**, 423–436 (2001).
47. F. Deschamps, L. Cobden, and P. Tackley, "The primitive nature of large low shear wave velocity provinces," Earth Planet. Sci. Lett. **349–350**, 198–208 (2012).
48. R. A. Duncan and R. A. Keller, "Radiometric ages for basement rocks from the Emperor Seamounts," Geochem. Geophys. Geosyst. **5** (2004). doi 10.1029/2004GC000704
49. C. J. Ebinger and N. S. Sleep, "Cenozoic magmatism throughout east Africa resulting from impact of a single plume," Nature **395**, 788–791 (1998).
50. W. Fjeldskaar, "Viscosity and thickness of the asthenosphere detected from the Fennoscandian uplift," Earth Planet. Sci. Lett. **126**, 399–410 (1994).
51. D. Forsyth and S. Uyeda, "On the relative importance of the driving forces of plate tectonics," Geophys J. R. Astron. Soc. **43**, 163–200 (1975).
52. Y. Fukao, S. Widiyantoro, and M. Obayashi, "Stagnant slabs in the upper and lower mantle transition region," Rev. Geophys. **39**, 291–323 (2001).
53. R. G. Gordon, "The plate tectonic approximation: Plate nonrigidity, diffuse plate boundaries, and global plate reconstructions," Annu. Rev. Earth Planet. Sci. **26**, 615–642 (1998).
54. S. P. Grand, R. D. van der Hilst, and S. Widiyantoro, "Global seismic tomography: A snapshot of convection in the Earth," GSA Today **7** (4), 1–7 (1997).
55. Y. Gung, M. Fanning, and B. Romanovicz, "Global anisotropy and the thickness of continents," Nature **422**, 703–711 (2003).
56. G. Hirth and D. Kohlstedt, "Rheology of the upper mantle and the mantle wedge: a view from the experimentalists," in *Inside the Subduction Factory*, Vol. 138 of *Geophys. Monogr. Ser.*, Ed. by J. Eiler (Am. Geophys. Union, Washington, D.C., 2003), pp. 83–105.
57. B. R. Julian, G. Foulger, O. Hateld, S. Jackson, E. Simpson, J. Einbeck, and A. Moore, "Hotspots in hindsight," *AGU Fall Meeting, San Francisco, United States, 2014* (Am. Geophys. Union, Washington, D.C., 2014), p. S51B–4468.
58. M. Lustrino and E. Sharkov, "Neogene volcanic activity of western Syria and its relationship with Arabian plate kinematics," J. Geodyn. **42**, 115–139 (2006).
59. S. Maruyama, M. Santosh, and D. Zhao, "Superplume, supercontinent, and post-perovskite: Mantle dynamics and anti-plate tectonics on the Core–Mantle Boundary," Gondwana Res. **11**, 7–37 (2007).
60. W. J. Morgan, "Convection plumes in the lower mantle," Nature **230**, 42–43 (1971).
61. A. Paulson, Sh. Zhong, and J. Wahr, "Modelling postglacial rebound with lateral viscosity variations," Geophys. J. Int. **163**, 357–371 (2005).
62. Yu. L. Rebetsky, "On small tangential mass forces that may exist in the lithosphere. Their role in tectonics and geodynamics," Geodyn. Tectonophys. **7**, 691–704 (2016).
63. G. Schubert, D. L. Turcotte, and P. Olson, *Mantle Convection in the Earth and Planets* (Cambridge Univ. Press, Cambridge, 2004).
64. W. D. Sharp and D. A. Clague, "50-Ma initiation of Hawaiian–Emperor Bend records major change in Pacific Plate motion," Science **313**, 1281–1284 (2006).
65. M. Stein and A. W. Hofmann, "Fossil plume head beneath the Arabian lithosphere," Earth Planet. Sci. Lett. **114**, 193–209 (1992).

66. J. Strehlau and R. Meissner, "Estimation of crustal viscosities and shear stresses from an extrapolation of experimental steady state flow data," in *Composition, Structure and Dynamics of the Lithosphere-Asthenosphere System*, Vol. 16 of *Geodyn. Ser.*, Ed. by K. Fuchs and C. Froidevaux (Am. Geophys. Union, Washington, D.C., 1987), pp. 69–87.

67. J. A. Tarduno, R. A. Duncan, D. W. Scholl, R. D. Cottrell, B. Steinberger, T. Thordarson, B. C. Kerr, C. R. Neil, F. A. Frey, M. Torii, and C. Carvallo, "The Emperor Seamounts: Southward motion of the Hawaiian hotspot plume in Earth's mantle," Science **301**, 1064–1069 (2003).

68. O. Tatar, J. D. A. Piper, H. Gürsoy, A. Heimann, and F. Koşbulut, "Neotectonic deformation in the transition zone between the Dead Sea Transform and the East Anatolian Fault Zone, southern Turkey: A paleomagnetic study of the Karasu Rift volcanism," Tectonophysics **385**, 17–43 (2004).

69. V. G. Trifonov, A. E. Dodonov, E. V. Sharkov, D. I. Golovin, I. V. Chernyshev, V. A. Lebedev, T. P. Ivanova, D. M. Bachmanov, M. Rukieh, O. Ammar, H. Minini, A.-M. Al Kafri, and O. Ali, "New data on the Late Cenozoic basaltic volcanism in Syria, applied to its origin," J. Volcanol. Geotherm. Res. **199**, 177–192 (2011).

70. V. P. Trubitsyn and M. N. Evseev, "Pulsation of mantle plumes," Russ. J. Earth Sci. **16** (2016). doi 10.2205/2016ES000569

71. V. P. Trubitsyn, M. N. Evseev, and A. P. Trubitsyn, "Influence of continents and lithospheric plates on the shape of D'' layer and the spatial distribution of mantle plumes," Russ. J. Earth Sci. **15** (2015). doi 10.2205/2015ES000552

72. J. T. Wilson, "A possible origin of the Hawaiian Islands," Can. J. Phys. **41**, 863–870 (1963).

Reviewers: V.V. Yarmolyuk, E.P. Dubinin

Translated by E. Maslennikova